Appl Phys A (2009) 94: 73–82
DOI 10.1007/s00339-008-4939-7

Applied Physics A
Materials Science & Processing

The influence of nitridation time on the structural properties of GaN grown on Si (111) substrate

Engin Arslan · Mustafa K. Ozturk · Özgür Duygulu · Ali Arslan Kaya · Suleyman Ozcelik · Ekmel Ozbay

Received: 31 July 2008 / Accepted: 13 October 2008 / Published online: 30 October 2008
© Springer-Verlag 2008

Abstract In the present paper, the effect of in-situ substrate nitridation time on crystalline quality of GaN films grown on Si (111) substrates by metal organic chemical vapor deposition (MOCVD) were investigated. A thin buffer layer of silicon nitride (SiN_x) with various thicknesses was achieved through the nitridation of substrate at different nitiridation times ranging from 0 to 660 s. The structural characteristics, such as dislocation densities, correlation lengths of columnar crystallites, the tilt and twist of the mosaic structure, and the angles of rotational disorder, were all studied in detail by using a planar and cross-sectional view of high resolution transmission electron microscopy (HRTEM) and X-ray diffraction (HRXRD) performed at different scattering geometries. It was found that the dislocation densities, lateral coherence lengths, vertical coherence lengths, and the tilt and twist of mosaic blocks in GaN films monotonically varies with the nitridation time. The experimental findings showed that the nitridation times had more influence on edge dislocation densities than the screw type.

PACS 61.05.Cp · 61.72.Uj · 64.70.Kg · 68.37.Lp · 68.37.Og · 72.80.Ey · 78.55.Cr

E. Arslan (✉) · E. Ozbay
Nanotechnology Research Center, Department of Physics, Department of Electrical and Electronics Engineering, Bilkent University, Bilkent, 06800 Ankara, Turkey
e-mail: engina@bilkent.edu.tr
Fax: +90-312-2901015

M.K. Ozturk · S. Ozcelik
Department of Physics, Faculty of Science and Arts, Gazi University, Teknikokullar, 06500 Ankara, Turkey

M.K. Ozturk
Department of Mineral Analysis and Technology, MTA, 06520 Ankara, Turkey

Ö. Duygulu
TUBITAK Marmara Research Center, Materials Institute, P.O. Box 21 Gebze Kocaeli, 41470, Kocaeli, Turkey

A.A. Kaya
Engineering Faculty, Metallurgy and Materials Eng. Dept., Mugla University, 48170 Mugla, Turkey

1 Introduction

The large direct band-gap and good thermal stability properties of the GaN and related materials has enabled their potential use in applications for laser diodes (LDs), visible-blind ultraviolet (UV) detectors, and short-wave light-emitting diodes (LEDs) [1–4]. However, there is still a lack of a suitable substrate for GaN-based devices to fully exploit their superior properties. Thus far, there have been a large number of studies concerned with the growth of GaN films on highly lattice-mismatched substrates, such as sapphire [5], SiC [6], or Si [7]. Among these materials, silicon has many advantages compared to SiC and sapphire due to its high crystal quality, low cost, good electrical and thermal conductivity, and large-area size as a substrate for the growth of GaN, AlGaN epitaxial layers [8, 9].

However, the growth of GaN films on a Si wafer is usually associated with such problems as cracking in the epitaxial layer because of large mismatches in the lattice parameters (−16.9%) and thermal expansion coefficients (approx. 113%) [5, 7, 10–13]. Due to a large lattice mismatch, a high density of threading dislocations on the order of (10^9–10^{10} cm^{-2}) exists in the GaN film on silicon substrates, which significantly affects the performance of the

GaN based devices [8]. In order to obtain crack-free high-quality GaN film on Si substrate, various types of buffer layers and growth conditions as well as post-growth heat treatment processes have been proposed by different research groups [10–17]. However, the appearance of the cracks is quite random on the film, which produces significant difficulty in device applications. Therefore, the control of crack distribution for a large area film is the main issue of the present study [7–11].

It has been recently demonstrated that defect-free GaN on Si could be realized when a Si_xN_y buffer was used in hot wall chemical vapor deposition [14] with MOCVD [15] growth techniques. These buffer layers were achieved by nitridating the Si substrate with N_2 flow at 900°C by Huang et al. [14] and at 1120°C by Wu-Yih Uena et al. [15]. With a similar approach, a double-buffer structure of AlN/Si_xN_y was used to obtain high quality GaN film on Si substrate by using molecular beam epitaxy (MBE) [16]. The single-crystalline SiN_x was obtained by introducing the active nitrogen plasma to the Si (111) surface at 900°C for approximately 30 s. Hageman et al. [17] reported significant improvements on the optical and structural properties of the 1 μm GaN layer with the creation of a SiN_x intermediate layer.

Large lattice mismatch with respect to the substrate commonly causes high dislocation densities in heteroepitaxial thin films [18–21]. These types of structures are often described by the model of mosaic crystals [20, 22]. The lateral and vertical dimensions of the crystallites are given by the lateral and vertical coherence length. The angular mismatch of the crystallites causes a tilt and twist, describing the angular distribution of the crystallographic orientation of the mosaic blocks perpendicular to, and within, the growth plane. Knowledge of all these structural parameters in detail is crucial in order to understand the microstructural properties of the grown epilayers, to optimize the growth conditions, and the buffer design for better GaN film quality on Si substrate.

We investigated in detail the effect of in-situ substrate nitridation time (assumed to cause an SiN_x amorphous interlayer) on the characteristics of structural features (correlation lengths that are normal and parallel to the substrate surface, tilt and twist, and heterogeneous strain) by HXRD, and the interface structure of $AlN/SiN_x/Si$ (111) and the dislocation densities (edge and screw types) by both TEM and XRD. The nitridation time varied from 0 to 660 s.

2 Experimental procedure

GaN epitaxial layers on Si (111) substrate were grown in a low-pressure MOCVD reactor (Aixtron 200/4 HT-S). The reactant source materials for Ga, Al, and N were trimethylgallium (TMGa), trimethylaluminum (TMAl), and NH_3, respectively. The H_2 was used as a carrier gas during AlN and GaN growth. Before loading, the Si substrates were sequentially degreased by H_2SO_4:H_2O_2:H_2O (2:1:1) solutions for 1 min, and etched while in a 2% HF solution for 1 min, rinsed in de-ionized water, and dried with a nitrogen gun. At the beginning of the growth of AlN, the substrate was baked in an H_2 ambient at 1100°C for 10 min to remove the native oxide. To grow a SiN_x interlayer on a Si (111) substrate surface, following the thermal etching, the substrate was nitridated by exposing it to the NH_3 flow of 0.900 slm at 1020°C. Nitridation was performed at five different times. The nitridation times were: 0 (without nitridation), 10, 60, 120, 420, and 660 s for samples A, B, C, D, E, and F, respectively. After the nitridation, for all the samples, we grew an approximately 150 nm high-temperature (1100°C) AlN (HT-AlN) buffer layer. In all of the samples, the 250 nm GaN layers were grown at 1050°C. For sample A, in order to prevent the growth of an amorphous SiN_x interlayer, the technique of the Al pre-covering process of Si substrate was applied before the growth of the AlN buffer.

The crystalline quality of the GaN layers was examined by high resolution X-ray diffraction (HRXRD). The X-ray diffraction was performed using a Bruker D-8 high-resolution diffractometer system, delivering a CuKα1 (1.540 Å) radiation. Data were collected on the (0002), (0004), (0006), $(10\bar{1}5)$, $(20\bar{2}2)$, $(12\bar{3}1)$, $(10\bar{1}1)$, $(10\bar{1}3)$, and $(11\bar{2}4)$ reflections.

HRTEM (High Resolution Transmission Electron Microscopy) was used to correlate the X-ray measurements to the microstructure, crystal structure, and dislocations of c-plane GaN grown with SiN_x interlayer. TEM examinations were conducted on the plan-view and cross-sectional samples.

For the cross-sectional TEM investigations, all the samples were prepared via a conventional sandwich technique, i.e., mechanically thinning them to a thickness of approx. ∼5 μm by dimple grinding. Gatan 691 Precision Ion Polishing System (PIPS) was used to prepare the thin foils.

The specimens were examined by using a JEOL 2100 High Resolution Transmission Electron Microscope (LaB_6 filament) operated at 200 kV.

3 Results and discussion

Figure 1 shows the typical 2θ scan X-ray diffraction (XRD) patterns of the GaN films grown on a nitridated (with 120 s nitridation time) Si (111) substrate. As shown in Fig. 1, the diffraction patterns only exhibited the dominant Wurtzite GaN crystalline (0002) peaks plus (0002) peaks from the AlN layer and (111) peaks from Si substrate. This indicates the hexagonal structure of the GaN epilayer with its [0001] direction parallel to the [111] of Si substrate. For sample D, the (0002) reflections of Wurtzite GaN are clearly observed at 17.162° and the (111) peak from Si substrate at 17.161°, respectively.

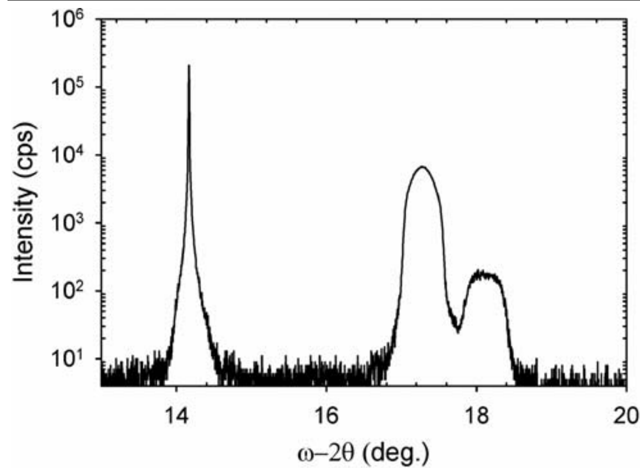

Fig. 1 An HR-XRD $\omega - 2\theta$ scan pattern obtained using four-Ge (022) crystal monochromotor from a GaN epilayer grown on Si (111) substrate with 120 s nitridation times (sample D)

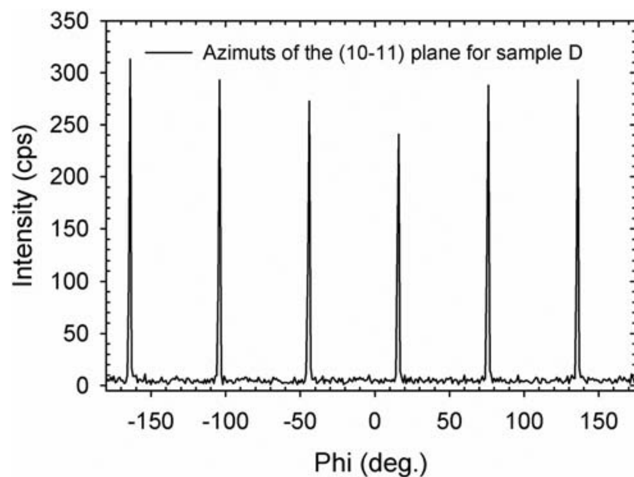

Fig. 2 Phi-scan curve of asymmetric GaN $(10\bar{1}1)$ reflection plane for sample D. Every peak shows the azimuths of the $(10\bar{1}1)$ plane. The diffractive peak repeats every 60°

An in-plane Φ-scan was also taken by rotating the sample around its surface-normal direction in order to investigate the in-plane alignment of GaN film. Figure 2 shows the Φ-scan pattern of the $(10\,\bar{1}1)$ plane of sample D. It can be seen in Fig. 2 that the diffraction peaks from the $(10\,\bar{1}1)$ plane of GaN were observed at 60° intervals, which clearly confirms the good single crystal hexagonal structure of the GaN epilayer.

The influence of the nitridation time on the structural properties of a GaN epilayer

Heteroepitaxial thin films with a large lattice-mismatch with respect to the substrate in turn form a mosaic structure of slightly misoriented sub-grains [18, 19, 22], which is characterized by the nucleation of slightly misoriented islands and the coalescence of these islands towards a smooth surface. The mosaic structure of the epilayers is determined by the size and angular distribution of the mosaic blocks. The vertical and lateral correlation lengths, heterogeneous strain, and degree of mosaicity as expressed by the tilt and twist angles are important parameters in characterizing the quality of the epitaxial films with a large lattice mismatch to the substrate [17, 19, 22]. The mosaic blocks are assumed to be slightly misoriented with respect to each other. The out-of-plane rotation of the blocks perpendicular to the surface normal is the mosaic tilt, and the in-plane rotation around the surface normal is the mosaic twist. The average absolute values of tilt and twist are directly related to the full width at half maximum (FWHM) of the corresponding distributions of the crystallographic orientations [18, 23].

The parameters of the vertical and lateral coherence length and tilt angle can be obtained from the Williamson–Hall measurement, and the twist angle from an approach, which was developed by Srikant et al. [23] or from direct measurement [24], which explains the superposed effect of the tilt and twist on the broadening of the full-widths at half-maximum (FWHMs) of the off-axis plane rocking curves [25].

Each contribution to the broadening of the particular XRD curves can be separated in the Williamson–Hall measurement [18, 25]. Specifically, in triple-axis diffractometer measurements, the broadening of the rocking curve (angular-scan or ω-scan) of the symmetric (0002), (0004), and (0006) reflections for the GaN epitaxial layer is influenced only by the tilt angle α_{tilt} and short coherence length parallel to the substrate surface $L_{\parallel}$.

Separation analogous of the tilt angle α_{tilt} and short coherence length can be made with the Williamson–Hall plot, when $\beta_{\Omega}(\sin\theta)/\lambda$ is plotted against $(\sin\theta)/\lambda$ for each reflection and fitted by a straight line. Then, the tilt angle α_{tilt} is obtained from the slope of the linear dependence, and lateral coherence length $L_{\parallel}(L_{\parallel} = 0.9/(2y_0))$ from the inverse of the y-intersection y_0 of the fitted line with the ordinate, where β_{Ω} is the FWHM in angular unit, θ is the Bragg reflection angle, and λ is the X-ray wavelength.

In the radial-scan direction ($\omega - 2\theta$-scan) of the symmetric reflections (0002), (0004), and (0006), a small vertical correlation length and a heterogeneous strain along the c-axis causes a broadening of the Bragg reflections. This two parameters $L_{\perp}$ and $\varepsilon_{\perp}$ can similarly be derived from the Williamson–Hall plot. The $L_{\perp}$ and $\varepsilon_{\perp}$ parameters can be derived from the $\beta_{2\theta-\Omega}(\cos\theta)/\lambda$ against $(\sin\theta)/\lambda$ plots for each reflection.

Figure 3 shows the corresponding Williamson–Hall plots for reflections (0002), (0004), and (0006) for the triple-axis (a) ω-scan and (b) $\omega - 2\theta$ of all the samples with different nitridation times. The straight lines are linear fits of the experimental data. The expected linear behavior of the graphs

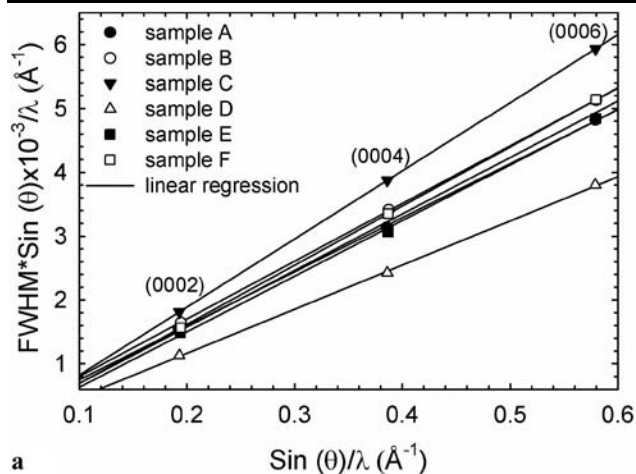

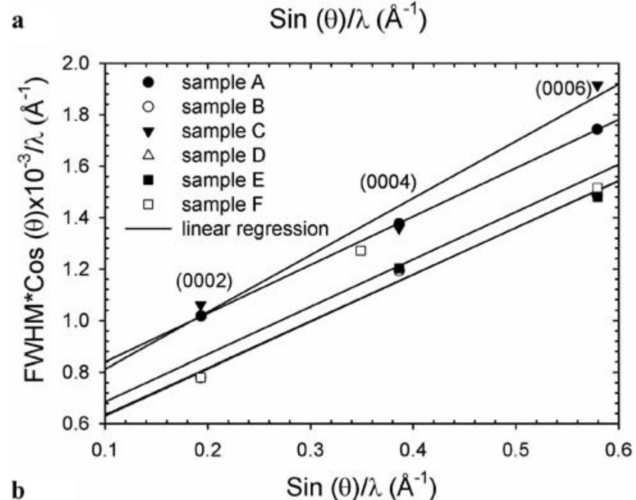

Fig. 3 Williamson–Hall plot for the GaN layers without nitridation and with different nitridation times. (**a**) Triple-axis ω scan and (**b**) triple-axis $\omega - 2\theta$ scan were measured for the $(000l)$ $(l = 2, 4, 6)$ reflections indicated in the figure. The lines result from a linear fit of the data

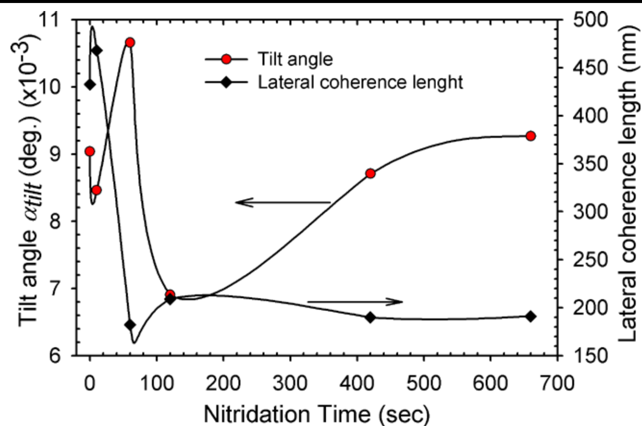

Fig. 4 Tilt and lateral coherence length obtained from the Williamson–Hall plot as a function of the nitridation time

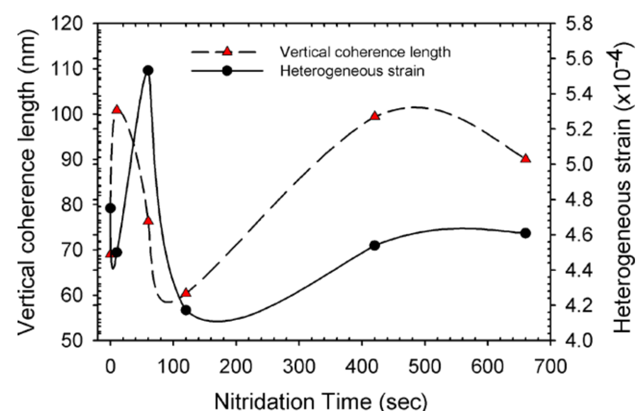

Fig. 5 Vertical coherence length and heterogeneous strain obtained from the Williamson–Hall plot as a function of the nitridation time

is experimentally well confirmed, which gives rather accurate tilt angle values.

The lateral coherence lengths and tilt angles are shown in Fig. 4. As can be seen, the tilt angles for all the samples were rather small. It can be seen in the figure that, as the nitridation times increased, the tilt angles decreased first and then increased to 10.6×10^{-3} degrees for sample C (60 s). From these nitridation times, we can see small increments in the tilt angle. The minimum tilt angle was obtained for sample D. The lateral coherence lengths were determined to range from 182 to 467 nm. As seen in Fig. 4, as the nitridation times increased the $L_{\parallel}$ increased first and then decreased. The maximum values were observed for the nitridation times of 10 s (sample B).

The vertical coherence lengths $L_{\parallel}$ values are shown in Fig. 5. Its values range from 60 to 100 nm. It can be seen in Fig. 5 that there is an increment in all the samples except for sample D.

The strain normal to the substrate $\varepsilon_{\perp}$ values, which was obtained for all the samples, is shown in Fig. 5. The $\varepsilon_{\perp}$ values range from 4.2×10^{-4} to 5.5×10^{-4}. Small changes were observed for a heterogeneous strain with the nitridation time length.

The mean twist angle between the subgrains can be extrapolated from a fit to the measured double-axis scans data for different (hkl) reflections in the skew symmetric diffraction. Several extrapolation methods have been reported in the literature for the mean twist angle calculation [18, 23, 26]. However, all of these methods include a complicated calculation and fitting procedure for the extraction of the twist angle from the experimental data. On the other hand, Zheng et al. [24] proposed a simple empirical approach to obtain the mean twist angle directly without falling into complications.

The FWHM of the rocking curve of an imperfect film is composed of several contributions, such as the mean tilt, twist, the average size of sub-grains, and inhomogeneous strain distributions. Although the broadening, which is due to a limited domain size and an inhomogeneous strain, can

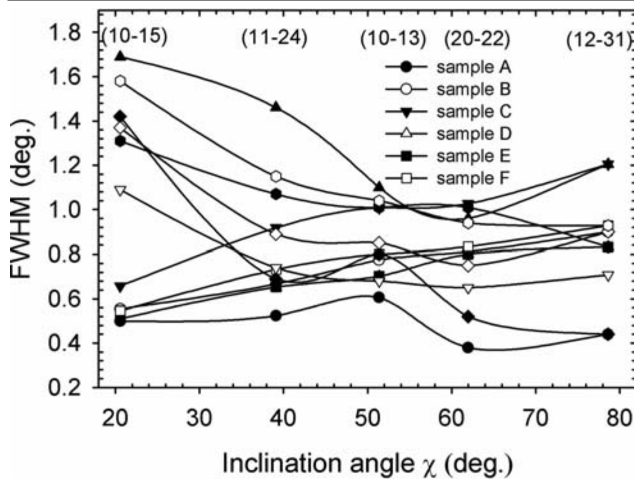

Fig. 6 FWHM values of the rocking curves of Φ and ω scans for (hkl) reflections (marked in the figure) vary with the inclination angle χ for all of the samples. FWHMs of Φ scan increase with the increment of χ angle, while those of ω scan decrease. The lines are a guide for the eyes

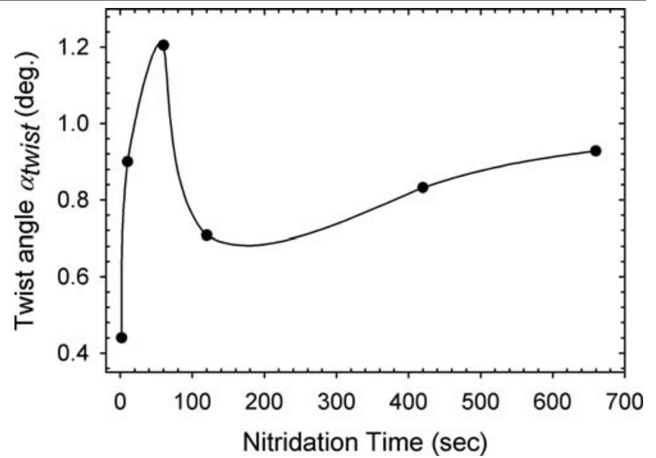

Fig. 7 The dependence of the twist angle on the nitridation time

be significant in highly imperfect films, their effects have been eliminated by the use of a slit of 0.6 mm placed in front of the detector in double-axis ω-scans. Indeed, their contribution to the overall broadening was found to be of minor influence in this measurement case.

In addition, the (0002) reflection and (hkl) reflections with h or k non-zero orientation of our samples with triple-axis $\omega - 2\theta$-scans both exhibit a small FWHM. The last important point is that the intrinsic width of the reflection for the crystal and the apparatus broadening for all the experimental reflections are negligible because these effects amount to only a few arcsec. For this reason, we can only measure the broadening that is caused by the twist by using (hkl) reflections in the skew geometry.

The extended FWHMs of ω and Φ-scans that were obtained by using the fit of the Pseudo-Voigt function to the rocking curves are shown in Fig. 6 as a function of increasing χ for all the samples. It can be seen in Fig. 6 that the FWHMs of ω and Φ-scans are nearly the same when the inclination angle is 78.6°. In this inclination angle, the $(12\bar{3}1)$ reflection appears. These results showed that the rocking-curve widths of ω or Φ scans for this higher χ angle are close to the twist angles. In every respect, the FWHMs of Φ-scans are larger than those of the χ-scans with the change of the inclination angle χ. Therefore, the mean twist angles must be the average value of the FWHMs of the ω and Φ-scans of $\chi = 78.6°$.

The measured mean twist angle of the GaN layers is shown in Fig. 7 as a function of the nitridation time. The mean twist angle is strongly dependent on the nitridation time. The minimum mean twist angle value was obtained as 0.4° for sample A (without nitridation). It increases with the nitridation time and reaches to a maximum value of 1.2° for sample C (with 60 s nitridation) and then decreases to 0.7° for sample D (with 120 s nitridation) nitridated the longest. Based on this observation, it can be argued that the mean twist angle of the GaN epilayers that are grown on Si substrate is strongly affected by the time elapsed for the nitridation of the substrate before intiating GaN growth.

There are three main types of dislocations present in GaN thin film that are grown on Si (111) with two steps [7–16, 18, 24, 27]: the pure edge dislocation with Burgers vector $b = \frac{1}{3}\langle 11\bar{2}0\rangle$ ($\langle a\rangle$), the pure screw dislocation with Burgers vector $b = \langle 0001\rangle$ ($\langle c\rangle$), and the mixed dislocation with $b = \frac{1}{3}\langle 11\bar{2}3\rangle$ ($\langle c + a\rangle$). The coherence lengths, and the twist and tilt are correlated with the different types of dislocations. As reported by Metzger et al. [18], for (0002)-oriented GaN epitaxial films, the mean twist angle is monotonically related to the density of edge-type of the threading dislocation (TD) with Burgers vector $b = 1/3\langle 11\bar{2}0\rangle$, while the mean tilt angle is monotonically related to, and can be converted into, the density of the screw-type of TD with Burgers vector $b = \langle 0001\rangle$. Thus, in the present study, all the existing dislocation lines were treated as the types defined by Metzger et al. [18].

The screw dislocation ($b = \langle 0001\rangle$) density (D_{screw}) can be calculated from the equation [28, 29],

$$D_{\mathrm{screw}} = \frac{\alpha_{\mathrm{tilt}}^2}{4.35|b_{\mathrm{screw}}|^2}, \tag{1}$$

where α_{tilt} is the tilt angle, and b is the Burgers vector length ($b_{\mathrm{screw}} = 0.5185$ nm).

The edge type dislocations with Burgers vector ($b = \frac{1}{3}\langle 11\bar{2}0\rangle$) reconcile an azimuthal rotation of crystallites around the surface normal. From the measured twist angle α_{twist}, an edge-type dislocation density can be calculated. If dislocations are piled up in small angle grain boundaries,

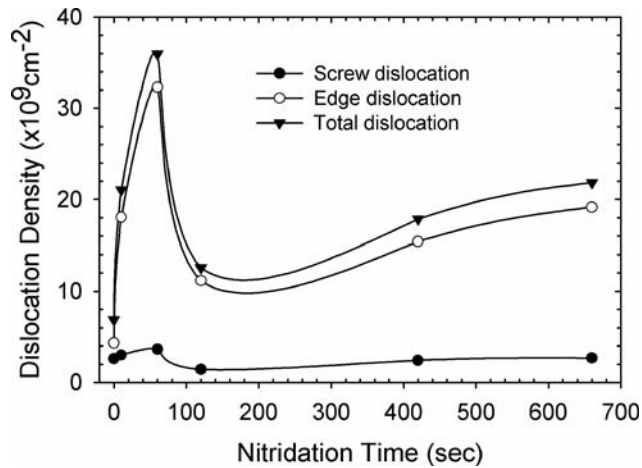

Fig. 8 The edge, screw, and total dislocation density as a function of the nitridation time

the edge dislocation density (D_{edge}), therefore, can be calculated according to [28, 29],

$$D_{\text{edge}} = \frac{\alpha_\phi}{2.1|b_{\text{edge}}|L_\parallel}, \tag{2}$$

where b is the Burgers vector length ($b_{\text{edge}} = 0.3189$ nm). Figure 8 shows the edge, screw, and total dislocation density as a function of nitridation time length. As can be seen from this figure, the edge and screw dislocation densities are approximately equal to each other for sample A (without nitridation). The edge dislocation density changed with the nitridation times. On the other hand, the screw dislocation densities approximately keep constant for all the nitridation times. These results show that the nitridation process is much more effective on the edge type dislocation density.

The microstructure of the grown layers was revealed by TEM. The cross-sectional and plan-view TEM specimens were prepared from the grown layers. In Fig. 9(a), we show the cross-sectional TEM images of the GaN films grown on Si (111) with a 660 s nitridated buffer layer (sample F). The GaN-AlN and Si were viewed in the $[1\bar{1}00]$ and $[11\bar{2}]$ projections, respectively. A relatively rough interface between the HT-AlN nucleation layer and GaN, and a high density of threading dislocations (TD) can be clearly observed. From Fig. 9(a), it can be seen that, the dislocation density decreases rapidly within 50 nm from the AlN/GaN interface into the GaN layer. Since dislocations cannot end within a crystal, that is, the ends of a dislocation can only be at free surfaces, or at interfaces, the apparent change in the dislocation density within the GaN layer requires an explanation. The dislocations originating from the GaN/AlN interface may change direction and bend back to the interface that they originate from. Tilt or twist boundaries that are said to exist within the GaN layer may also assist in such changes in dislocation directions. Some studies even suggest the presence of small angle grain boundaries with the GaN layer [18]. The wavy nature of the AlN/GaN interface may also be related to the tilt and twist boundaries in the GaN layer.

Other aspects requiring explanation are the crystallographic relationship between the AlN layer and Si substrate, as well as the apparent stress that consequently also leads to the observed high dislocation density within the AlN layer. If the interface was truly between the AlN and Si substrate, the crystallographic relationship and relatively high dislocation density, originating from the interface due to the large lattice mismatch between the two crystals, would provide a straightforward explanation. However, the AlN/Si interface has been shown, in the present study and others, to contain an amorphous SiN_x layer [34, 36, 37]. The orientation relationships were determined for GaN-AlN on Si (111) by taking the selected area electron diffraction (SAED) patterns in TEM (Fig. 9(b) and Fig. 10(b), (c)). It is noteworthy that despite the presence of an amorphous SiN_x interlayer, the selected area electron diffraction (SAED) confirms the well-known orientation relationships between GaN (AlN) and Si [34], which are $\langle 11\bar{2}0\rangle_{\text{GaN}}$ // $\langle 11\bar{2}0\rangle_{\text{AlN}}$ // $\langle 1\bar{1}0\rangle_{\text{Si}}$,$\langle 1\bar{1}00\rangle_{\text{GaN}}$ // $\langle 1\bar{1}00\rangle_{\text{AlN}}$ // $\langle 11\bar{2}\rangle_{\text{Si}}$, and $\langle 0001\rangle_{\text{GaN}}$ // $\langle 0001\rangle_{\text{AlN}}$ //$\langle 111\rangle_{\text{Si}}$. By this, it has also been proven that GaN and AlN have hexagonal crystal structures and are single crystals.

Several reports have addressed the issue of a crystallographic relationship between AlN and Si despite the amorphous SiN_x between them. One of the suggestions was that the amorphous SiN_x layer has some short range order that necessitates the orientation of the AlN layer in this fashion [34]. According to some others, there exists in the SiN_x a top layer of a few atomic distances that is crystalline [36]. According to Dobos et al. [37], Nakada et al. [36], and Kaiser et al. [34], the epitaxial relationship is transferred from Si into AlN and GaN through the amorphous SiN_x layer by the presence of crystalline regions, Si_3N_4 inclusions, or holes in the SiN_x layer. Other explanations include the short-range tetrahedral coordination that was maintained in the SiN_x layer [34, 41, 42], and the nucleation and growth of GaN islands from intrinsic or extrinsic defects by a "pinhole model" [40].

In our view, perhaps the most plausible explanation is that the amorphous SiN_x layer is not continuous and that there must be some points of actual contact between the crystalline Si substrate and deposited AlN layer [40]. It is then conceivable to assume that such locations of contact would inevitably behave like seeds in bulk single crystal growth techniques in turn leading to an overall crystallographic relationship between AlN and Si despite the presence of an intermittent amorphous SiN_x. If such a mode of deposition is operational, then the large lattice mismatch between AlN and Si in the locations of true contact could also act as a source for dislocation emissions, and thereby explain the

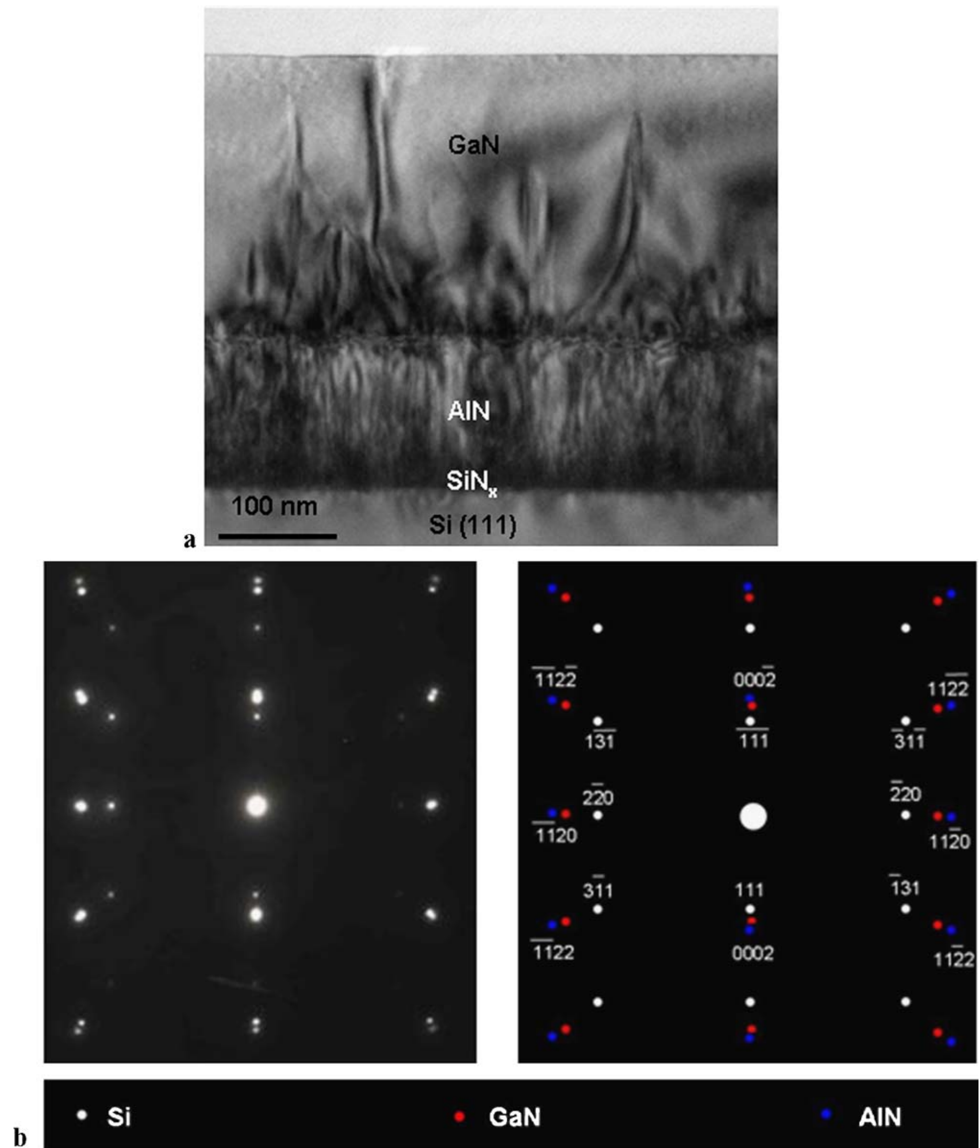

Fig. 9 (**a**) Cross-sectional Bright Field TEM image, and (**b**) corresponding diffraction pattern for GaN-AlN [1$\bar{1}$00] zone axis and Si [11$\bar{2}$] zone axis

high dislocation density within AlN. Our observations on the cross sections taken from different locations of the same sample showed that SiN_x is indeed intermittent. It may further be suggested that the tilt and twist boundaries that are said to exist in GaN may also be related to the growth modes of the AlN layer.

In addition to the arguments mentioned above, the crystal orientation of the hexagonal AlN with the basal planes parallel to its interface with the substrate may also arise from the simple thermodynamic requirement of lowering the surface energy. As a thin film and, therefore, having its largest surfaces parallel to the substrate it should be expected that AlN with a hexagonal crystal structure would, unless otherwise dictated by a crystalline substrate, prefer to form outer surfaces out of densely packed, i.e., low energy, basal planes. Therefore, even if no effect was imposed by the amorphous SiN_x for a particular orientation relationship, a free-growing AlN layer would be expected to position itself in the observed fashion, i.e., basal planes parallel to the substrate.

A plain AlN film on Si contains a large number of dislocations due to the strain relaxation of the film [30]. Follstaedt et al. [31] and Datta et al. [32] have demonstrated that, plan-view TEM imaging is generally accepted as a more trustworthy method for TD density measurement, compared to other techniques, such as atomic force microscopy (AFM) and cathodoluminescence (CL). These techniques cannot be used effectively to detect a-type edge dislocations that thread to the film surface, since such dislocations do not create steps on the surface that are detectable by AFM, and are probably not effective nonradiative recombination centers that are detectable by CL [31–34].

The threading dislocations (TD) density of sample F (with 660 s nitridation) was determined by plan-view TEM. The plan-view image of sample F is shown in Fig. 10(a). All

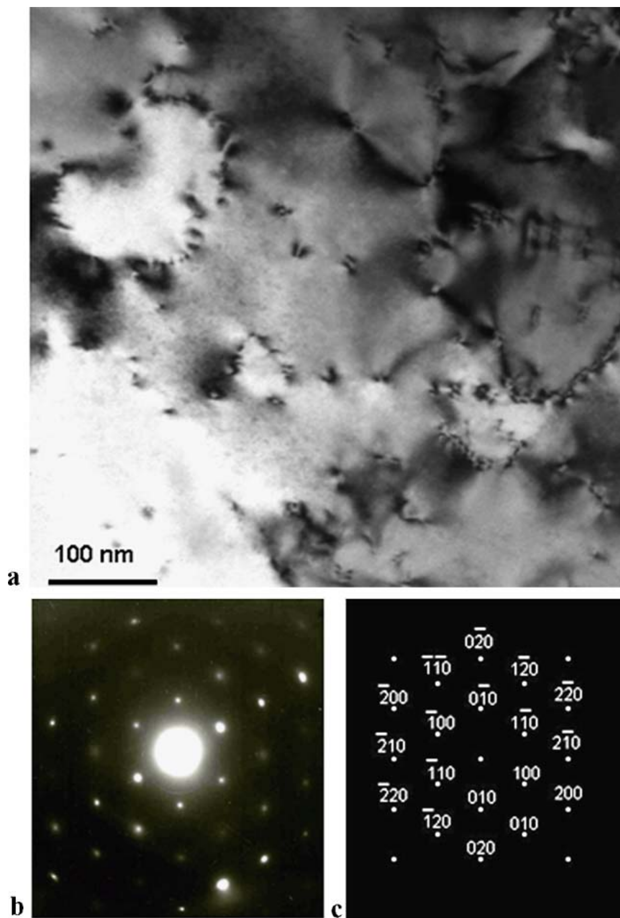

Fig. 10 (**a**) Plan-view TEM micrographs of the GaN layer on the AlN nucleation overlayer grown with the insertion of an SiN_x layer (sample F) and (**b**) corresponding diffraction pattern, and (**c**) indexed sketch of the basic reflections for the GaN [0001] zone axis

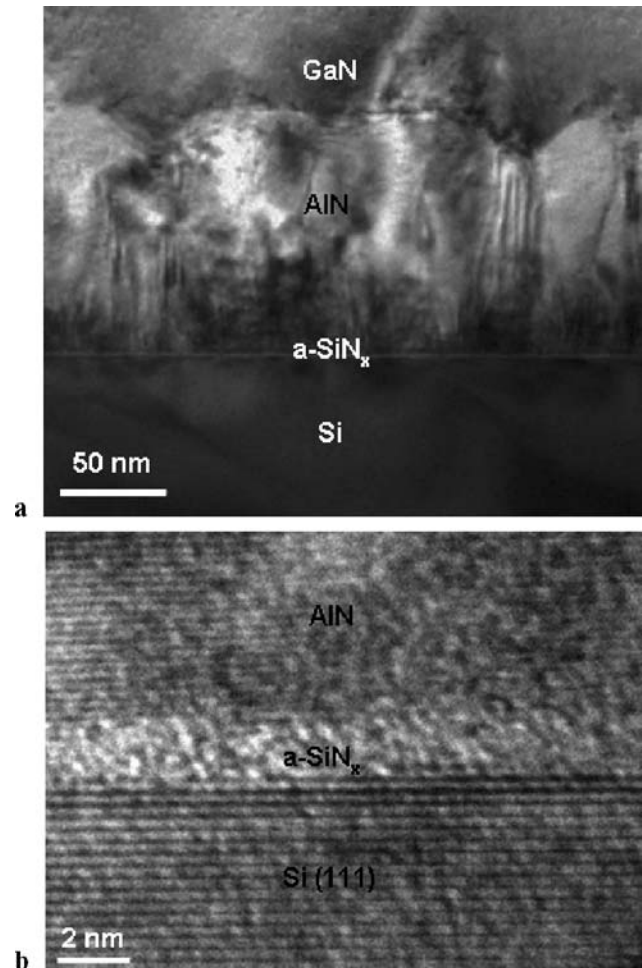

Fig. 11 (**a**) Low-magnification and (**b**) HRTEM image of the Si/AlN interface with the a-SiN_x intermediate layer

of the images were bright-field (BF) images which were collected by using multi-beam diffraction conditions. The plan-view specimens were investigated in the [0001] zone-axis orientation, which were nearly in the optical axis. The determined values are characteristic for the near surface region, only (∼top 100 nm). Moreover, the crystal defects, which were revealed by cross-sectional studies, did not propagate to the surface, and are not visible in the plan-view images [30, 34, 35].

As shown in Fig. 10(a), a network structure of defect arrays was also observed. The image shows that the dislocations in the epitaxial layers are not uniformly distributed. In order to determine the TD densities, the number of TDs was counted for approximately 10 different plan-view TEM images similar to those shown in Fig. 10. All of the images, for TD density determination, were collected with their GaN [0001] zone axis. The density of these threading dislocations was approximately 9×10^9 cm^{-2}, which is comparable to the values that were calculated with the HR-XRD measurements.

Between the Si substrate and AlN layer, a thin layer (∼ 2 nm) was observed (Fig. 11). From the cross-sectional High Resolution TEM (HRTEM) image (Fig. 11(b)) for sample F it is observed that this thin layer is amorphous SiN_x (a-SiN_x). This a-SiN_x is also observed in several Si/AlN systems [33, 34, 36–42].

Cross-sectional HRTEM images are shown for the GaN/AlN interface in Fig. 12. A rough interface is observed mostly for the GaN/AlN layers (Fig. 11(a) and Fig. 12(a)). However, smoother interface segments were also observed in some regions (Fig. 12(b), (c)).

From the SAED results, with the epitaxial relation, it can be observed that the crystal orientation of Si (111) seems to be transferred mostly through the amorphous SiN_x into the AlN and GaN layers. One reason could be the short-range tetrahedral coordination of each atom, which is obviously continued in the SiN_x layer. Another explanation could be small crystalline SiN or Si_3N_4 within the interlayer, which transfer the orientation relation [34, 36]. Secondly, a locally, thicker SiN_x layer in the structures can cause the interrup-

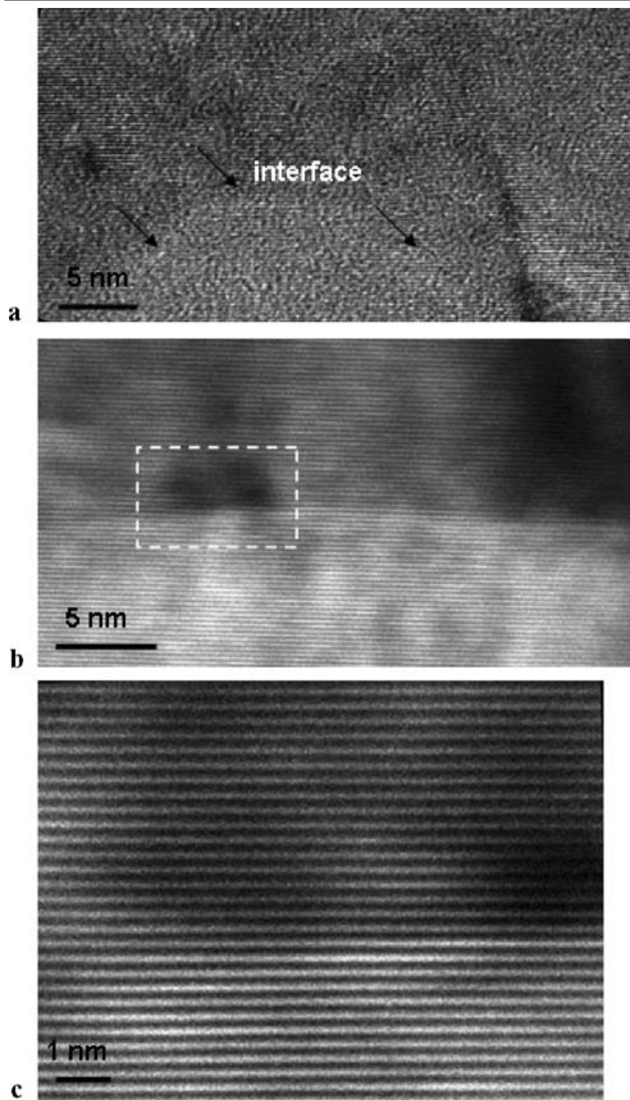

Fig. 12 (**a**) HRTEM image of the rough AlN/GaN interface shown by the *arrows*, (**b**) HRTEM image of the smoother AlN/GaN interface region, and (**c**) magnified view of the selected region of (**b**)

tion of the crystal symmetry transfer. For this reason, we obtained (0002) orientated AlN grains (Fig. 9) with slightly tilted grains. In our present study, it was important to avoid an excessively large SiN_x layer thickness that would totally interrupt the transfer of the epilayer relation from the Si (111) substrate to the epitaxial layer and that would cause a polycrystalline deposition of GaN, as given by other growth process [13–16, 31, 33–35].

4 Conclusions

In the present study, the influence of in-situ substrate nitridation time (assumed to cause an SiN_x amorphous interlayer) on the characteristics of the structural features by HXRD, and the interface structure of AlN/SiN_x/Si (111) and dislocation densities (edge and screw types) were investigated by both TEM and XRD measurements of the hexagonal epitaxial GaN films grown on Si (111). The nitridation time lengths ranged from 0 to 660 s. The mosaic structure of the GaN layers was affected by the nitridation time length. We obtained the largest values for vertical and lateral coherence length at 10 s nitridation. On the other hand, when the Si (111) was not nitridated, the smallest twist angle was obtained (sample A). The smallest tilt angle of a 6.9×10^{-3} degree was obtained for the 120 s nitridated sample. From the dislocation measurements, we can see that the edge type dislocation densities are much more affected from the nitridation process. However, screw dislocation densities are less affected by nitridation. From the SAED results, with the epitaxial relation, it can be observed that the crystal orientation of Si (111) seems to be transferred mostly through the amorphous SiN_x into the AlN and GaN layers. However, it is important to avoid an excessively large SiN_x layer thickness, which would totally interrupt the transfer of the epilayer relation from the Si (111) substrate to the epitaxial and would cause the polycrystalline deposition of GaN.

Acknowledgement This work is supported by the European Union under the projects EU-METAMORPHOSE, EU-PHOREMOST, EU-PHOME, and EU-ECONAM, and TUBITAK under Project Numbers 105E066, 105A005, 106E198, 106A017, and 107A012. One of the authors (E.O.) also acknowledges partial support from the Turkish Academy of Sciences.

References

1. S.N. Mohammad, A. Salvador, H. Morkoç, Proc. IEEE **83**, 1420 (1996)
2. L. Shen, S. Heikman, B. Moran, R. Coffie, N.-Q. Zhang, D. Buttari, I.P. Smorchkova, S. Keller, S.P. DenBaars, U.K. Mishra, IEEE Electron Device Lett. **22**, 457 (2001)
3. S. Butun, M. Gokkavas, H. Yu, E. Ozbay, Appl. Phys. Lett. **89**, 073503 (2006)
4. T. Tut, M. Gokkavas, B. Butun, S. Butun, E. Ulker, E. Ozbay, Appl. Phys. Lett. **89**, 183524 (2006)
5. H. Yu, D. Caliskan, E. Ozbay, J. Appl. Phys. **100**, 033501 (2006)
6. R. Gaska, J.W. Yang, A. Osinsky, Q. Chen, M. Asif Khan, A.O. Orlov, G.L. Snider, M.S. Shur, Appl. Phys. Lett. **72**, 707 (1998)
7. A. Dadgar, C. Hums, A. Diez, J. Bläsing, A. Krost, J. Cryst. Growth **297**, 279 (2006)
8. S. Pal, C. Jacob, Bull. Mater. Sci. **27**, 501 (2004)
9. A. Krost, A. Dadgar, Mater. Sci. Eng. B **93**, 77 (2002)
10. M.-H. Kim, Y.-G. Do, H.C. Kang, D.Y. Noh, S.-J. Park, Appl. Phys. Lett. **79**, 2713 (2001)
11. Z.L. Fang, S.P. Li, J.C. Li, H.Z. Sun, S.J. Wang, J.Y. Kang, Thin Solid Films **516**, 6344 (2008)
12. K. Cheng, M. Leys, S. Degroote, B. Van Daele, S. Boeykens, J. Derluyn, M. Germain, G. Van Tendeloo, J. Engelen, G. Borghs, J. Electron. Mater. **35**, 592 (2006)
13. S. Raghavan, J.M. Redwing, J. Appl. Phys. **98**, 023514 (2005)
14. J. Huang, Z. Ye, L. Wang, J. Yuan, B. Zhao, H. Lu, Solid-State Electron. **46**, 1231 (2002)

15. W.-Y. Uena, Z.-Y. Li, S.-M. Lan, S.-M. Liao, J. Cryst. Growth **280**, 335 (2005)
16. C.-L. Wu, J.-C. Wang, M.-H. Chan, T.T. Chen, S. Gwo, Appl. Phys. Lett. **83**, 4530 (2003)
17. P.R. Hageman, S. Haffouz, V. Kirilyuk, A. Grzegorczyk, P.K. Larsen, Phys. Stat. Sol. (a) **188**, 523 (2001)
18. T. Metzger, R. Höppler, E. Born, O. Ambacher, M. Stutzmann, R. Stömmer, M. Schuster, H. Göbel, S. Christiansen, M. Albrecht, H.P. Strunk, Philos. Mag. A **77**, 1013 (1998)
19. B. Heying, X.H. Wu, S. Keller, Y. Li, D. Kapolnek, B.P. Keller, S.P. DenBaars, J.S. Speck, Appl. Phys. Lett. **68**, 643 (1995)
20. M.E. Vickers, M.J. Kappers, R. Datta, C. McAleese, T.M. Smeeton, F.D.G. Rayment, C.J. Humphreys, J. Phys. D Appl. Phys. **38**, 99 (2005)
21. N.G. Weimann, L.F. Eastman, J. Appl. Phys. **83**, 3656 (1998)
22. V. Holy, J. Kubena, E. Abramof, K. Lischka, A. Pesek, E. Koppensteiner, J. Appl. Phys. **74**, 1736 (1993)
23. V. Srikant, J.S. Speck, D.R. Clarke, J. Appl. Phys. **82**, 4286 (1997)
24. X.H. Zheng, H. Chen, Z.B. Yan, Y.J. Han, H.B. Yu, D.S. Li, Q. Huang, J.M. Zhou, J. Cryst. Growth **255**, 63–67 (2003)
25. G.K. Williamson, W.H. Hall, Acta Metall. **1**, 22 (1953)
26. Y.J. Sun, O. Brandt, K.H. Ploog, J. Mater. Res. **18**, 1247 (2003)
27. H. Sasaki, S. Kato, T. Matsuda, Y. Sato, M. Iwami, S. Yoshida, J. Cryst. Growth **298**, 305 (2007)
28. P. Gay, P.B. Hirsch, A. Kelly, Acta Metall. **1**, 315 (1953)
29. C.G. Dunn, E.F. Koch, Acta Metall. **5**, 548 (1957)
30. H. Lahreche, P. Vennegues, B. Beaumont, P. Gibart, J. Cryst. Growth **205**, 245 (1999)
31. D.M. Follstaedt, P.P. Provencio, N.A. Missert, C.C. Mitchell, D.D. Koleske, A.A. Allerman, C.I.H. Ashby, Appl. Phys. Lett. **81**, 2758 (2002)
32. R. Datta, M.J. Kappers, J.S. Barnard, C.J. Humphreys, Appl. Phys. Lett. **85**, 3411 (2004)
33. X. Weng, S. Raghavan, J.D. Acord, A. Jain, E.C. Dickey, J.M. Redwing, J. Cryst. Growth **300**, 217 (2007)
34. S. Kaiser, M. Jakob, J. Zweck, W. Gebhardt, O. Ambacher, R. Dimitrov, A.T. Schremer, J.A. Smart, J.R. Shealy, J. Vac. Sci. Technol. B **18**(2), 733 (2000)
35. F. Wu, S. Zamir, B. Meyler, J. Salzman, Y. Golan, J. Electron. Mater. **31**, 88 (2002)
36. Y. Nakada, I. Aksenov, H. Okumura, Appl Phys Lett. **73**, 6951 (1998)
37. L. Dobos, B. Pécz, E. Feltin, B. Beaumont, P. Gibart, Vacuum **71**, 285 (2003)
38. M.-H. Kim, Y.-C. Bang, N.-M. Park, C.-J. Choi, T.-Y. Seong, S.-J. Park, Appl. Phys. Lett. **78**, 2858 (2001)
39. A. Chakraborty, K.C. Kim, F. Wu, J.S. Speck, S.P. DenBaars, U.K. Mishra, Appl. Phys. Lett. **89**, 041903 (2006)
40. M. Tamura, M. López-López, T. Yodo, Superficies Vacío **13**, 80 (2001)
41. Z. Fang, Surf. Coat. Technol. **202**, 4198 (2008)
42. Z.L. Fang, J.Y. Kang, W.J. Huang, H.T. Sun, M. Lu, J.F. Kong, W.Z. Shen, J. Phys. Chem. C **112**, 4925 (2008)